



# Flow feature and mixing performance analysis of RB-TSAR and EB-TSAR micromixers

Ranjitsinha R. Gidde<sup>1</sup> · Prashant M. Pawar<sup>1</sup>

Received: 29 April 2019 / Accepted: 21 May 2019 / Published online: 28 May 2019  
© Springer-Verlag GmbH Germany, part of Springer Nature 2019

## Abstract

Three-dimensional CFD simulations carried to evaluate mixing performance of two designs of micromixers namely RB-TSAR and EB-TSAR. The results of flow physics analysis indicate that the interfacial area between the two flow fluids can be enhanced by creating a flow in transverse direction with the help of split and recombination of fluid streams by placing baffles in diffuser shaped mixing elements along the axial direction. Further, the simulation results indicate that at inlet Reynolds number below 1, the molecular diffusion is the most dominant mechanism of mixing, and the mixing index is almost the same for all cases. However at  $Re > 5$ , the secondary flow influencing the mixing process dramatically and thus mixing index is increased. The results also reveal that baffles can break the fluid streams, produce fluid convection and increase the contact area of the fluid by folding and deflecting which in turn helps to improve the mixing index. The split and recombination of the fluid streams and separation vortices play vital role in enhancing the mixing performance. The design configurations studied here showed mixing index higher than 0.85 for the  $Re$  in the range from 10 to 50.

## 1 Introduction

In recent years, micromixer has been broadly used component in Lab-On-a-Chip and micro-total analysis systems ( $\mu$ TAS). Further, LOC and  $\mu$ TAS are used for biological analysis and chemical synthesis where rapid and efficient mixing is needed (Nguyen and Wu 2004; Hardt et al. 2004). Mixing is a critical issue for microfluidic application due to laminar flow regime with low Reynolds number. Mixing performance mainly relies on the molecular diffusion in laminar flow regime wherein the mixing process becomes time-consuming one (Bothe et al. 2006). There are three approaches to enhance the mass transfer in micromixers viz. improvement in the diffusion coefficient ( $D$ ), the concentration gradient of species ( $\nabla C$ ) and the interfacial surface area ( $A$ ) between different species of fluids. Out of these three methods, increasing the interfacial surface area between two different fluids in micromixers is considered to be an effective method for enhancing the mass transfer (Xia et al. 2016).

Various kinds of micromixers have been reported in previous studies to enhance mixing index, and to reduce the mixing time, the mixing length and the pressure drop. On the basis of external energy required to be provided to the micromixer or not, micromixers are generally classified into two types: active and passive micromixers. Active micromixers employs various methods, including dielectrophoresis (Goet et al. 2009), electrokinetic disturbance (Posner and Santiago 2006), pressure perturbation (Yaralioglu et al. 2004), magneto-hydrodynamic disturbance (Oh et al. 2007) and ultrasonic vibrations (Yang et al. 2000) to enhance mixing performance. However, due to the difficulties associated with the integration and fabrication of active micromixers (Chung et al. 2004) makes passive micromixers a smart alternative wherein no external energy source is required for moving the fluid through the microchannel.

Lamination and chaotic advection are two main mechanisms which are employed in passive micromixers for enhancing the mixing process. In lamination mechanism, the fluid is split into several laminar fluid streams and then recombined in order to increase the interfacial area between the fluids (Ansari and Kim 2010; Afzal and Kim 2012). Mixing efficiency can be remarkably improved by generating chaotic advection in the laminar flow by modifying the geometry of the microchannels (Kim et al. 2005;

✉ Ranjitsinha R. Gidde  
ranjitsinhag1@rediffmail.com

<sup>1</sup> SVERT's College of Engineering, Pandharpur,  
Maharashtra 413304, India

Suh and Kang 2010). To enhance mixing the optimization of the layout of obstacles in microchannels is carried out (Wang et al. 2002). A simple planar baffled micromixer with a short mixing distance has been designed for synthesis of nanoparticles (Chung et al. 2011). The effects of different types of wall protrusions on microfluidic mixing have been studied using CFD simulations (Sarkar et al. 2015). The effect of groove shape on mixing performance has been analyzed to find optimal groove shape for a pressure-driven flow across the microchannel. Numerous parametric studies were carried out to compare the optimal groove structure with other common groove type micromixers (Jain et al. 2013). CFD is reliable tool for both qualitative and quantitative analysis of flow structures, species concentration and mixing performance. Further, well-designed micromixer can reduce analysis time and size of footprint of a lab-on-a-chip system (Chen et al. 2016a, b; Gigras and Pushpavanam 2008). A planar passive micromixer with circular and square mixing chambers has studied recently (Gidde et al. 2018a). Fluid mixing in a swirl-inducing microchannel with square and T-shaped cross-sections has been studied for evaluating effect of shape and size of the channel cross-section on mixing performance (Huang et al. 2017). A numerical and experimental investigation has been performed to analyze the flow characteristics and mixing performance of four centrifuge-based compact disk microfluidic mixers with square-wave microchannels and different numbers and arrangements of inlet channels (Kuo and Li 2017). A study of a passive micromixer with lateral obstructions along a microchannel has been carried out to compare mixing efficiencies of micromixers with and without obstructions (Sahu et al. 2013). Numerical simulations have been performed to study and analyze the mixing performance of micromixers with serpentine microchannels. The results reveal that shapes of microchannels is a meaningful issue for improving the samples mixing index in passive micromixers (Chen et al. 2016a, b). The design optimization of rectangular wave micromixer (RWM) has been optimized using numerical simulations and Taguchi-based Grey Relational Analysis (GRA) (Gidde et al. 2018b). Taguchi method and numerical simulations have been employed to investigate the effect of geometry of micromixer on fluid mixing in micromixer having three mixing units (Shih and Chung 2008).

Numerical analysis and mixing experiments have been performed to investigate the mixing performance of SAR micromixers with E-shape mixing units. Further, micromixers showed an excellent mixing efficiency as a result of splitting-recombination and chaotic advection mechanisms (Chen and Shen 2017). Recently, flow feature analysis of an eye shaped split and collision (ES-SAC) element-based micromixer for lab-on-a-chip application

has been performed for mixing enhancement (Gidde et al. 2019). The mixing of fluids in wavy micromixer and wavy micromixer with obstacles on its side walls has been numerically investigated to compare performance with respect to mixing index, pressure drop, pumping power and performance index (Gidde and Pawar 2019). A planar three-rhombus micromixer with two constriction elements for good mixing has been demonstrated with the help of simulations and experiments (Chung and Shih 2007). Scalar mixing due to convection and diffusion in a microchannel mixer is studied using CFD. The effect of false diffusion is analyzed by a method which computes an average effective diffusivity in the numerical solution. This method is not limited to any particular numerical scheme, nor to any particular mesh type (Liu 2011).

The influence of the inlet flow conditions on the degree of mixing in a T-shaped micro-mixer has been investigated numerically. It has been observed that the flow nature at confluence for fully developed flow and not fully developed flow affects mixing efficiency (Galletti et al. 2012). The effects of various operating and design parameters on the mixing process in 3-D T-type micromixer have been investigated (Roudgar et al. 2012). An evaluation of mixing performance of convergent–divergent channel walls with sinusoidal variations has been carried out. The influence of the Reynolds number, the amplitude of the sinusoidal walls, and the aspect ratio of the channel on mixing performance is investigated (Afzal and Kim 2012). Numerical and experimental investigations on planar micromixers have been carried out to obtain an optimum micromixer with short mixing length (Cheri et al. 2013).

The 2-D Y-type micromixers and T-type micromixers have been systematically investigated based on fractal theory and generalized Murray's law. The effect of geometrical parameters on mixing efficiency and pressure drop was analysed (Chen et al. 2017). The layout optimization design of obstacles in a 3-D T-type micromixer was carried out. The orthogonal experiment method was applied for determining the effects of some key parameters on mixing efficiency (Chen and Zhao 2017). A passive planar micromixer with ellipse-like micropillars has been proposed to use in the laminar flow regime for high mixing efficiency (Tran-Minh et al. 2014). A micromixer with unbalanced three-split rhombic sub-channels has been analyzed for the mixing and flow characteristics (Hossain and Kim 2014). A novel micromixer design with shifted trapezoidal blades has been designed to obtain high mixing efficiency even at low Reynolds number (Re) based on the combination of several mixing principles, including vortices, transversal flows and chaotic advection (The et al. 2015a, b).

In the microchannel, the fluid moves through the channel at a constant rate due to the pressure gradient between

the inlet and the outlet. In such case, the channel geometry and obstacles affects degree of mixing. Looking to the advantages of split and recombine (SAR) mechanism for better mixing, the three inlet micromixers having diffuser shaped mixing elements and two types of baffles have been studied. Accordingly, for increasing the mixing index, two micromixer design configurations namely rectangular baffle based triple split and recombine (RB-TSAR) and elliptical baffle based triple split and recombine (EB-TSAR) having three inlets and diffuser shaped elements are presented.

## 2 Computational formulation

### 2.1 Micromixer design configuration

Figure 1 represents the schematic illustrations and geometrical details of RB-TSAR and EB-TSAR comprising three inlets, three baffles and three diffuser shaped mixing elements along the length of the microchannel. The inlets 1 and 2 are assigned to water, while inlet 3 is assigned to ethanol. In order to keep the same flow rate of two fluids, width of inlet 3 is kept twice the inlet 1 or Inlet 2 (i.e.  $W_e = 2W_w$ ). The detailed summary of all the dimensions is depicted in Table 1.

### 2.2 Governing equations

The CFD software COMSOL Multiphysics 5.0 was used to capture the flow and mixing field characteristics of the flow and mixing fields which has specific physics interfaces. The equations viz. continuity equation, momentum equation and convection diffusion equation were solved for incompressible, steady-state and laminar flow conditions (Okuducu and Aral 2018):

$$\nabla u = 0 \tag{1}$$

$$\rho \left[ \frac{\partial u}{\partial t} + (u \cdot \nabla)u \right] = -\nabla p + \mu \nabla^2 u \tag{2}$$

The mass transport in the case of the steady state in the three dimensional microchannel is governed by the convection–diffusion equation (The et al. 2015a, b).

$$\frac{\partial c}{\partial t} = D \nabla^2 c - u \cdot \nabla c \tag{3}$$

where  $u$  is the fluid velocity,  $p$  is the fluid pressure,  $\rho$  is the fluid density,  $\mu$  is the fluid viscosity,  $D$  is the diffusivity, and  $c$  is the molar concentration.

### 2.3 Boundary conditions

For numerical simulation study, water and ethanol were used as the fluid 1 and fluid 2 respectively and their physical properties are given in Table 2. Fluids were assumed to be incompressible and flow is assumed to be laminar. The boundary conditions of laminar inflow with

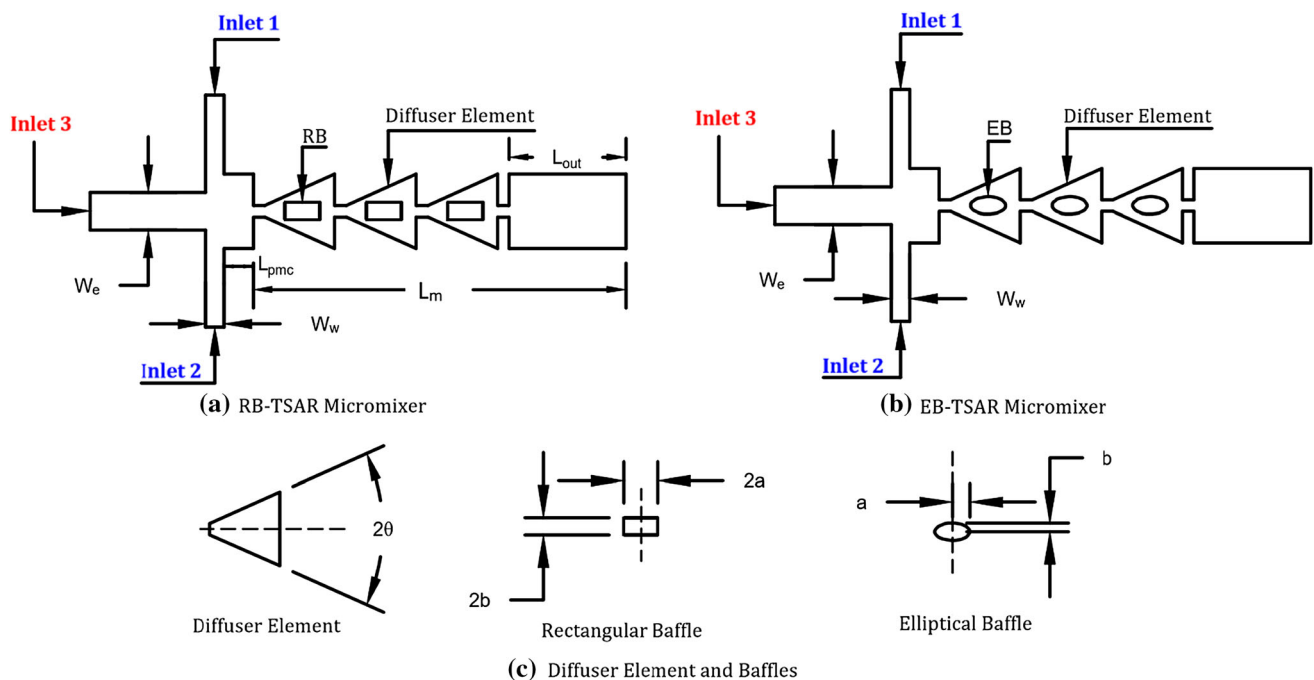


Fig. 1 Schematic illustrations of micromixer a RB-TSAR, b EB-TSAR and c diffuser element and baffles

**Table 1** Summary of dimensions of micromixer

Sr. No.	Parameter	Value	Unit
1.	Width of ethanol inlet ( $W_e$ )	160	$\mu\text{m}$
2.	Width of water inlet ( $W_w$ )	80	$\mu\text{m}$
3.	Length of premixing chamber ( $L_{pmc}$ )	125	$\mu\text{m}$
4.	Length of mixing channel ( $L_m$ )	1.6	mm
5.	Length of outlet channel ( $L_{out}$ )	500	$\mu\text{m}$
6.	Diffuser angle ( $2\theta$ )	12, 18, 24	$^\circ$ (degree)
7.	Length of rectangular baffle (2a)	150	$\mu\text{m}$
8.	Width of rectangular baffle (2b)	75	$\mu\text{m}$
9.	Semi-major axis of elliptical baffle (a)	75	$\mu\text{m}$
10.	Semi-minor axis of elliptical baffle (b)	37.5	$\mu\text{m}$
11.	No. of diffuser shaped elements	3	–
12.	No. of baffles	3	–

**Table 2** Properties of model fluids at 20 °C (Pradeep et al. 2016)

Property	Water	Ethanol
Density, $\rho$ in $\text{kg/m}^3$	$9.998 \times 10^2$	$7.89 \times 10^2$
Viscosity, $\mu$ in Pa.s	$0.900 \times 10^{-3}$	$1.20 \times 10^{-3}$
Diffusivity, $D$ in $\text{m}^2/\text{s}$	$1.200 \times 10^{-9}$	$1.20 \times 10^{-9}$

inlet flow velocities at the cross-section areas of channel inlets corresponding to inlet Reynolds number were employed to carry out simulations. The summary about flow velocity, Reynolds number and Peclet number is depicted in Table 3. Zero pressure boundary condition was set at the outlet. No-slip boundary condition was employed at the channel walls. The initial molar concentrations of water and ethanol were assumed to be 0.0 mol/L and 1.0 mol/L, respectively.

**Table 3** Flow velocity, Reynolds number and Peclet number

V (m/s)	Re	Pe
0.00012	0.1	84
0.00810	1	839
0.04090	5	4195
0.08180	10	8390
0.12270	15	12,585
0.16360	20	16,780
0.20450	25	20,976
0.24540	30	25,171
0.28630	35	29,366
0.32720	40	33,561
0.36810	45	37,756
0.40900	50	41,951

### 3 Performance characteristics

The performance characteristics viz. mixing index, pressure drop, performance index and mixing energy cost are vital in design of micromixer.

#### 3.1 Mixing index

The mixing index is used frequently to assess the quality of a device in mixing fluid processes. The mixing index is required to represent homogeneity, mixing quality of mixed fluid which in turn reflects the uniform degree of species concentration in the micromixer. It is based on the mass fraction standard deviation  $\sigma$  of one of the fluids at the channel outlet. The following expressions were used to determine mixing index (Hossain et al. 2017, Okuducu and Aral 2019):

$$\sigma^2 = \frac{1}{N_s} \sum_{i=1}^{N_s} (C_i - C_m)^2 \quad (4)$$

$$MI = 1 - \sqrt{\frac{\sigma^2}{\sigma_{max}^2}} \quad (5)$$

where  $N_s$  represents the number of sampling points on the cross-section plane under consideration;  $C_i$  and  $C_m$  represent the mass fraction of sampling point  $i$  and the optimal mass fraction, respectively.  $\sigma$  denotes the standard deviation of concentration and  $\sigma_{max}$  is the maximum standard deviation of concentration in the specific cross-section perpendicular to the flow direction. The brief summary of standard deviation, mixing index and species concentration which indicates mixing status is depicted in Table 4.

#### 3.2 Pressure drop

The pressure drop is another most important parameter in the LOC application apart from the mixing index. The

**Table 4** Mixing performance status

( $\sigma$ )	MI	C	Mixing status
$\sigma = \sigma_{\max}$	M = 0	$C_i = 0$	No mixing
$\sigma = 0$	M = 1	$C_i = C_m$	Full mixing

difference between the area weighted average of total pressure on the exit plane ( $P_o$ ) and on a cross-section plane at the inlet ( $P_i$ ) of the mixing channel is known as pressure drop (Cortes-Quiroz et al. 2009, 2014) and is directly related to the pumping power. The pressure drop is computed using Eq. (6) as given below:

$$\Delta P = P_i - P_o \tag{6}$$

For passive micromixers, the flow is driven by an applied pressure gradient. The greater driving force and more power are needed in case of high pressure drop. Consequently, the pressure drop must be considered together with mixing index in evaluating the overall performance and reliability of the micromixer.

### 3.3 Performance index

In order to evaluate the excellence of micromixer, performance index (ratio of mixing index to unit pressure drop) is vital one. High value of mixing index and low value of pressure drop are required to have a good performance index of a micro device (Gidde et al. 2018c)

$$PI = \frac{MI}{\Delta P} \tag{7}$$

where PI is performance index, MI is mixing index and  $\Delta P$  is the pressure drop.

### 3.4 Mixing energy cost

Characterizing the mixing performance of any micromixer design configuration, pumping power (power required to drive fluids through the channel or to run the whole micro device) and mixing index need to be considered concurrently. Commonly high mixing index at higher flow rates results in more power consumption (Falk and Commenge 2010; Ortega-Casanova 2016). So, it is important to determine the mixing energy cost (MEC) using Eq. (8) as given below:

$$MEC = \frac{\Delta P \times Q}{MI} \tag{8}$$

where  $\Delta P$  is the pressure drop in Pascal, Q is the corresponding flow rate ( $m^3/s$ ). It is expressed in Watts or  $\mu W$ .

## 4 Results and discussion

Computational Fluid Dynamics (CFD) results obtained at different Reynolds numbers were the basis for an in-depth flow physics analysis of micromixer. Further, which is used to understand mixing mechanism and to evaluate the micromixer design configurations in respect of performance characteristics viz. mixing index, pressure drop, performance index, and mixing energy cost.

### 4.1 Mixing field analysis

Verifying the grid independence of numerical simulation results is a vital factor that influences accuracy of the solution. Hence, in order to find out the optimal number of grids, the computational domain was discretized with hexahedral grids. Accordingly, five structured grid systems with hexahedral elements ranged from 1,08,433 to 2,44,273, were tested for SB-TSAR micromixer at Re of 50. Figure 2a shows hexahedral grid systems used for micromixers RB-TSAR. The summary about results of mixing index and pressure drop, detailed statics of grid elements and computed % error for grid dependency of RB-TSAR is depicted in Table 5. The error is estimated by using Eq. (9) (Xia et al. 2016).

$$\%error = \left| \frac{F_2 - F_1}{F_1} \right| \times 100 \tag{9}$$

where  $F_1$  is value of mixing index or pressure drop for the finest grids and  $F_2$  is value of mixing index or pressure drop for other grids. The % errors in results of mixing index and pressure drop of RB-TSAR micromixer with 1,92,896 and 2,44,273 grid elements are around 0.06 and 0.04 for mixing index and pressure drop, respectively. In addition, through the statics of grids, the average element quality and the maximum element quality of 1,92,896 hexahedral elements employed discretization computational domain of RB-TSAR micromixer are 0.4839 and 0.9521, respectively.

Therefore, grid system with minimum element size and maximum element size of 0.0004 mm and 0.0065 mm, respectively was selected to carry out further simulations for all the cases of the micromixers. Similarly, grid independence tests were conducted to identify the optimum grid system for EB-TSAR micromixer. The velocity profile on x–y plane at the half height of microchannel for RB-TSAR micromixer at Re = 50 is shown in Fig. 2b. The velocity magnitude decreases as fluid streams travel through diverging area and again increases when fluid stream forced in second constriction channel. The pressure contour results at Re = 50 obtained through simulation for RB-TSAR micromixer are shown in Fig. 2c. The comparison of the flow physics of mixing mechanism on x–y plane at half



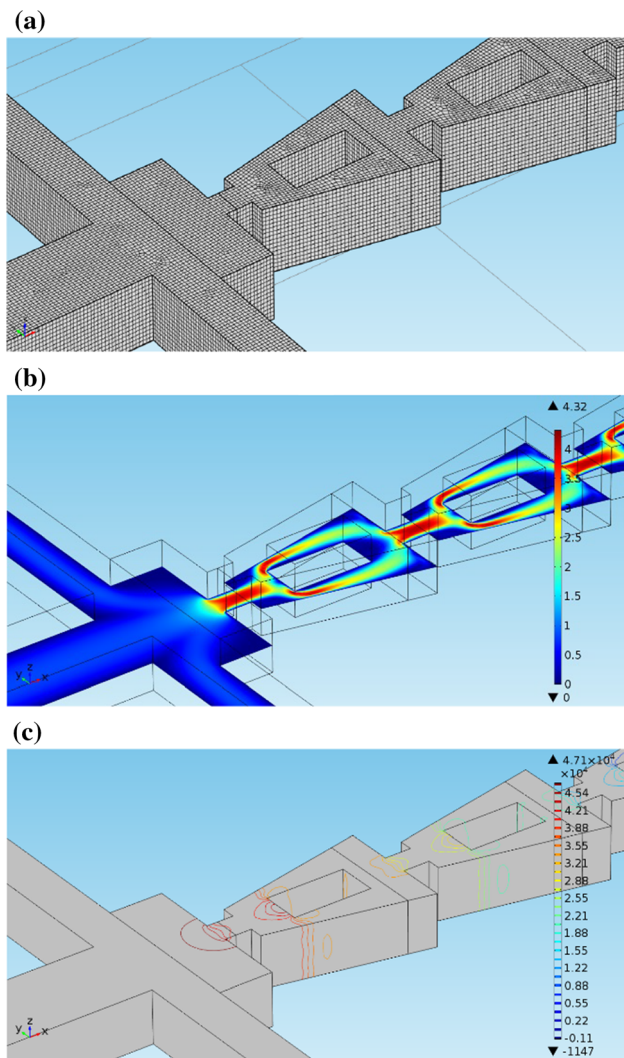


**Fig. 2** Mesh independency test **a** discretization of computational domain using 1,92,896 hexahedral elements, **b** velocity profile on  $x$ – $y$  plane and **c** pressure contours for RB-TSAR micromixer at  $Re = 50$

height of the channel with diffuser angle  $2\theta = 12^\circ, 18^\circ$  and  $24^\circ$  for  $Re = 15, 30$  and  $45$  is shown in Figs. 3 and 4 for RB-TSAR micromixer and EB-TSAR micromixer, respectively. As the two fluids enter the mixing unit, they

experience a diverging shape inside the mixing unit and baffle at the middle of the mixing element that leads splitting and recombination of fluid streams which creates a transverse motion of the fluids in the mixing channel and consequently improves fluid mixing.

The molar concentrations of the ethanol and water species are 1 and 0, respectively. The red color represents ethanol and the blue color represents pure water. Full mixing is obtained when the molar intensity of the two species becomes 0.5. The color of the fluid streams clearly varied with the increase in mixing distance and more intensified mixing can be observed in 3rd mixing element. It also indicates that the mixing performance becomes better with increase in  $Re$  due to the creation of strong vortices as a result of split and recombination of fluid streams. Furthermore, the mixing becomes more intensified with increase in the mixing region due to the increase in the diffuser angle from  $12^\circ$  to  $24^\circ$ .

For both RB-TSAR and EB-TSAR micromixers, mixing is characterized by the effects of separation and recombination as a result of shape of the mixing element and obstacles at the middle. The mixing enhancement is dominated by chaotic advection and its intensification is more at  $Re \geq 15$ . At  $Re \geq 15$ , the split and recombination of the fluid streams, Dean and separation vortices increase the interfacial area of the fluid streams as a result of convection and hence more mixing enhancement has been observed in both micromixers. The generation of Dean and separation vortices is due to the divergence section of the diffuser shaped mixing element and split and recombination mechanism of the fluids streams is due to the baffles. The strength of Dean and separation vortices is more in EB-TSAR as compared to the RB-TSAR. Hence more intensified mixing takes place in the EB-TSAR.

Mass fraction profiles at certain  $y$ – $z$  planes namely A–A, B–B, C–C, D–D, E–E and F–F at the Confluence Point, 0.12 mm, 0.4 mm, 0.75 mm, 1.1 mm and 1.7 mm, respectively for RB-TSAR micromixer and EB-TSAR micromixer are illustrated in Figs. 5 and 6, respectively. The color gradient between red and blue on  $y$ – $z$  plane

**Table 5** Grid independency test for RB-TSAR at  $Re = 50$

Grid system	G <sub>1</sub>	G <sub>2</sub>	G <sub>3</sub>	G <sub>4</sub>	G <sub>5</sub>
No-of elements	1,08,433	1,28,884	1,58,295	1,92,896	2,44,273
Element size (mm)					
Maximum	0.008000	0.007500	0.007000	0.006500	0.006000
Minimum	0.000550	0.000500	0.000450	0.000400	0.000350
Mixing index	1.000	0.985	0.9735	0.9721	0.9715
% error	1.50	1.17	0.14	0.06	–
Pressure drop (Pa)	48,800	48,200	47,980	47,920	47,900
% error	1.23	0.46	0.13	0.04	–
Comment				Optimal grid	

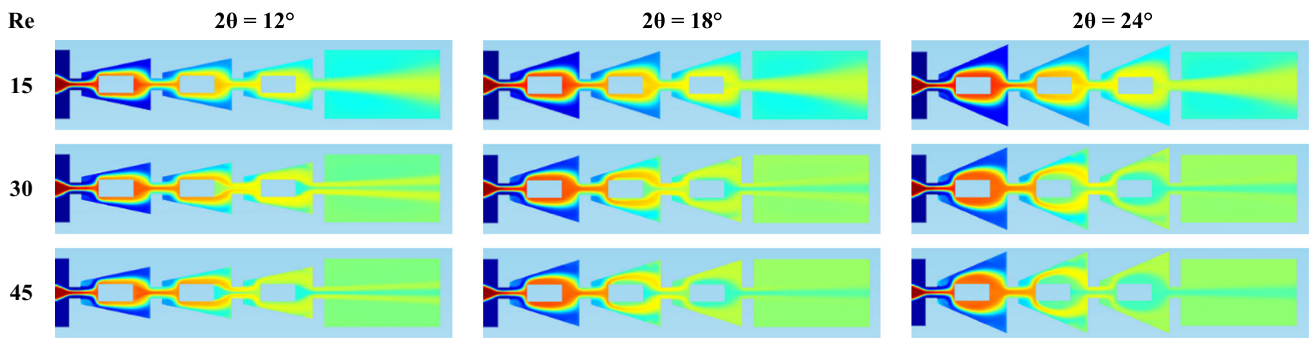


**Fig. 3** Ethanol mass fraction profiles on x–y plane at the middle of the height of the microchannel for RB-TSAR micromixers with divergence angle,  $2\theta = 12^\circ, 18^\circ$  and  $24^\circ$  for Reynolds numbers,  $Re = 15, 30$  and  $45$ , respectively

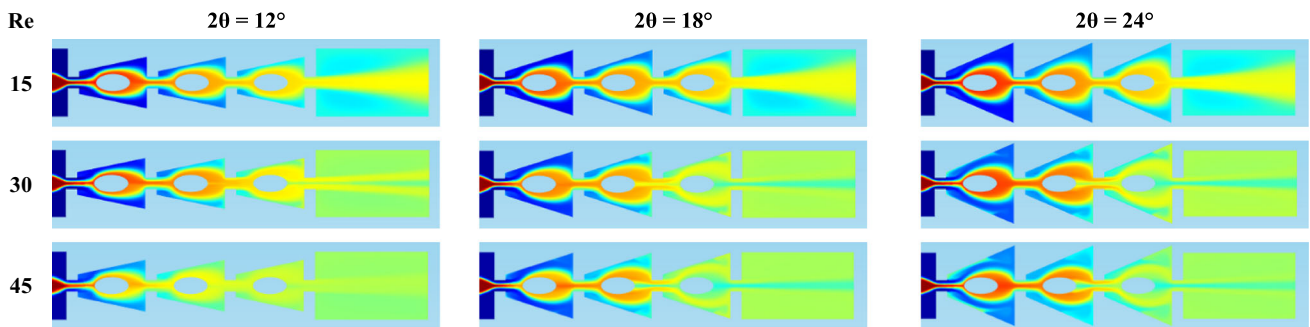


**Fig. 4** Ethanol mass fraction profiles on x–y plane at the middle of the height of the microchannel for EB-TSAR micromixers with divergence angle,  $2\theta = 12^\circ, 18^\circ$  and  $24^\circ$  for Reynolds numbers,  $Re = 15, 30$  and  $45$ , respectively

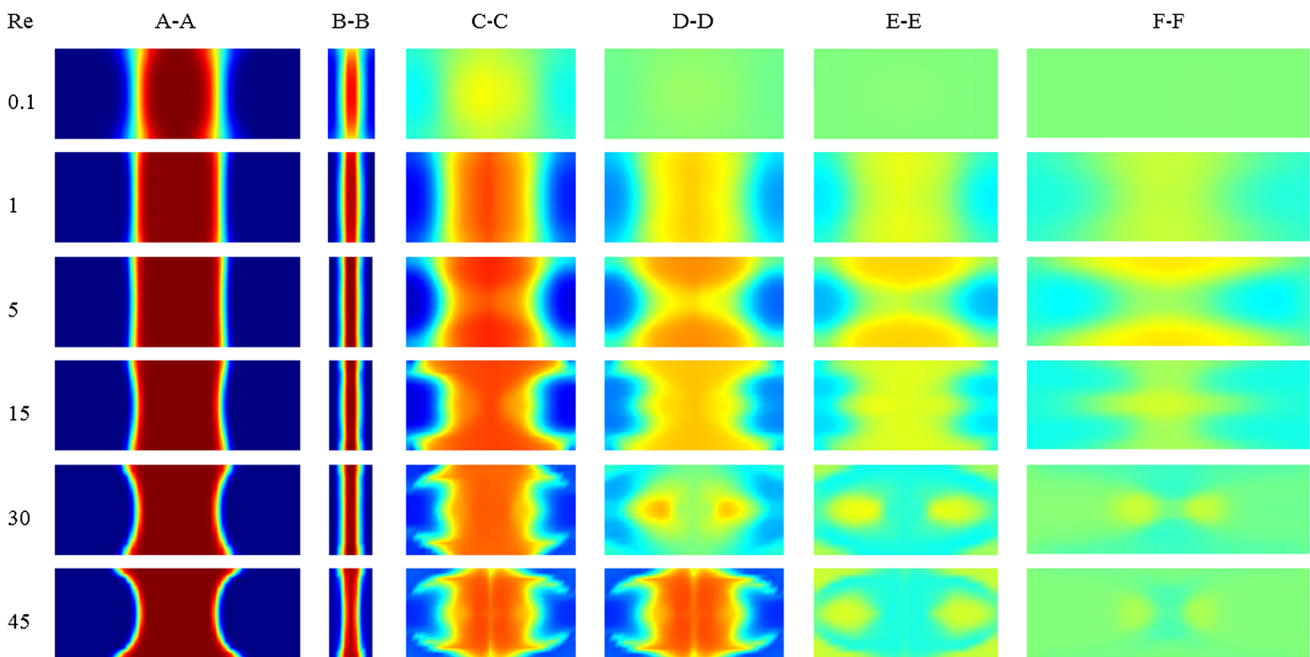


**Fig. 5** Ethanol mass fraction profiles on six cut planes for RB-TSAR micromixers with divergence angle,  $2\theta = 12^\circ$  for Reynolds numbers,  $Re = 0.1, 1, 5, 15, 30$  and  $45$ , respectively

indicates the degree of mixing, and a uniform mass fraction i.e. green color contour across the mixer outlet indicates thorough mixing. At  $Re = 0.1$ , the fluid interface distortion

is minimal when the fluids pass each diffuser shaped mixing element, and not much fluid splitting and recombination has been observed for RB-TSAR and EB-TSAR

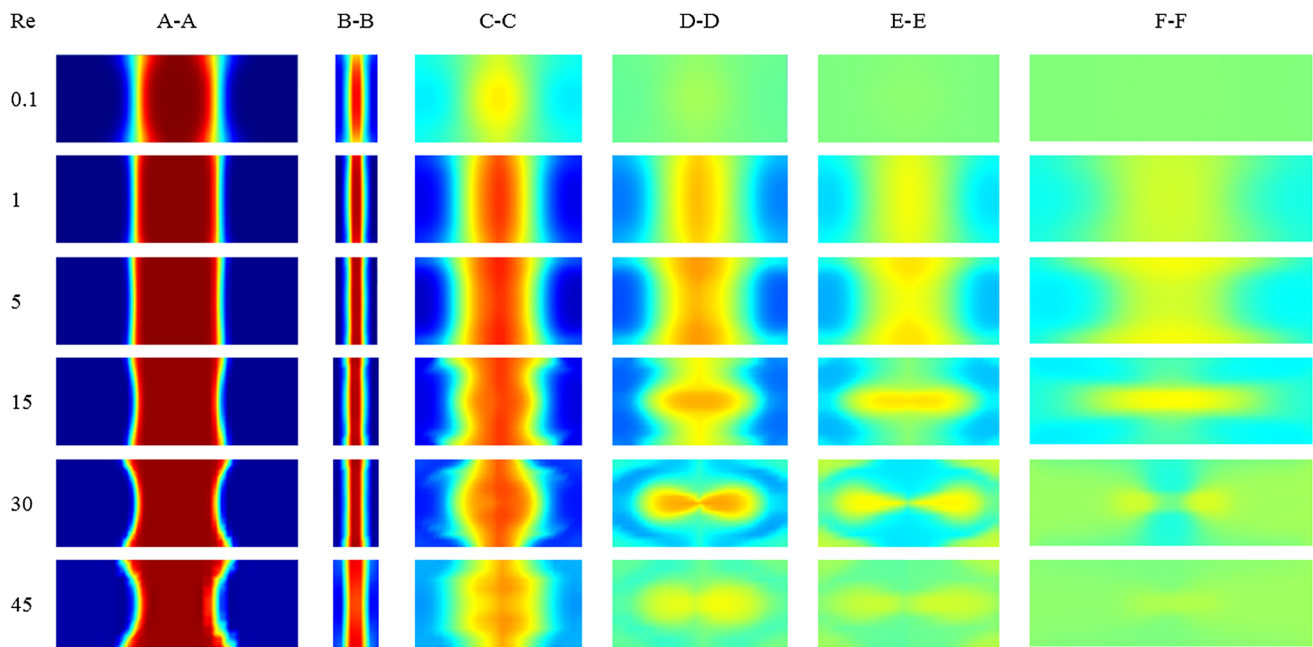


**Fig. 6** Ethanol mass fraction profiles on six cut planes for EB-TSAR micromixers with divergence angle,  $2\theta = 12^\circ$  for Reynolds numbers,  $Re = 0.1, 1, 5, 15, 30$  and  $45$ , respectively

micromixers. The enhancement in mixing is diffusion dominated. Increased residence time enhance diffusion dominated mixing while short residence increases the magnitude of the convection process (Shah et al. 2019). However at  $Re = 1$ , obvious distortion in fluid interface has been observed due to the more splitting and recombination of fluid streams. It can be realized from the mass fraction contour at the various planes that the transverse motion of the fluid becomes significant, especially at the top and bottom portions of the channel close to the walls as a result of increase in Reynolds number.

At  $Re > 5$ , the inertia force overwhelms viscous force and dominates the flows in the micro channels and this effect further increases with increase in Reynolds number. As the fluid flows proceeds through the diffuser elements, the transverse flow caused by split and recombination of fluid streams and divergence shape of the diffuser, Dean and separation vortices are produced. This is due to the baffles which stir up the fluid rapidly and increases the interfacial area of the two fluids, and reduced the diffusion path in the transverse direction. The results also reveal that baffles can break the fluid streams, produce fluid convection and increase the contact area of the fluid by folding and deflecting which in turn helps to improve the mixing index.

Hence, the MI higher than 0.80 for the  $Re > 5$  and the same can be visualized from the Figs. 3 and 5, and Figs. 4 and 6, respectively for RB-TSAR and EB-TSAR micromixers. The more intensification has been observed as flow travels over in the forward direction. Further, the

shape of baffles has influence on the flow physics or flow features of the mixing mechanisms as well as on the mixing enhancement as seen from six  $y$ - $z$  planes along the length of micromixer as shown in Figs. 7 and 8 for RB-TSAR micromixer and EB-TSAR micromixer, respectively. Figure 9 represents velocity field and velocity magnitude for both designs of micromixer with  $2\theta = 24^\circ$  for Reynolds numbers viz. 15, 30 and 45.

It is noticed that the shape of the baffle has significant influence on velocity field, velocity magnitude and flow features as shown in Fig. 9. On the basis of nature of flow feature after the baffle, it can be seen that the fluid flow travels in circular path in case of EB-TSAR as a result of curved profile of elliptical baffles and fluid travels in triangular path in case of RB-TSAR as result of sharp corners of the rectangular baffles. Thus, the fluid flow through EB-TSAR micromixer experiences less resistance in case as compared to RB-TSAR micromixer.

## 4.2 Analysis of performance characteristics

### 4.2.1 Mixing index

The mixing indices on  $y$ - $z$  planes at the exit were calculated. The influence of Reynolds number (range 0.1–50) on mixing index RB-TSAR and EB-TSAR is as shown in Fig. 10.

This performance is characterized by different mixing mechanisms such as split and recombine due to baffles, separation vortices and chaotic advection due to secondary



**Fig. 7** Ethanol mass fraction profiles on six planes for RB-TSAR with divergence angle,  $2\theta = 12^\circ$  for  $Re = 45$

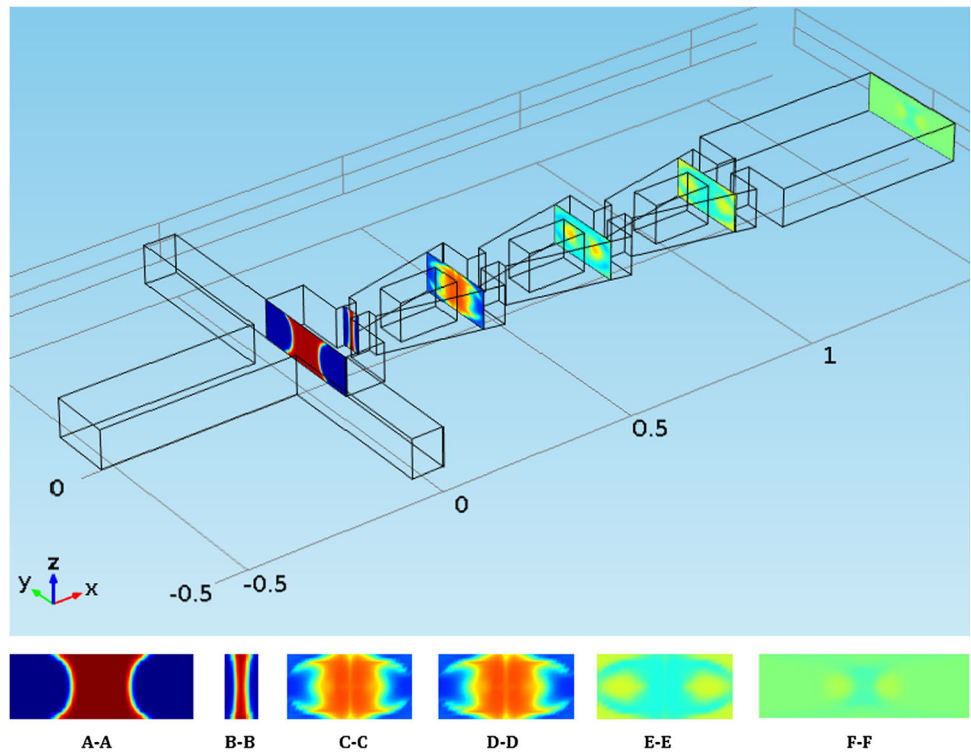
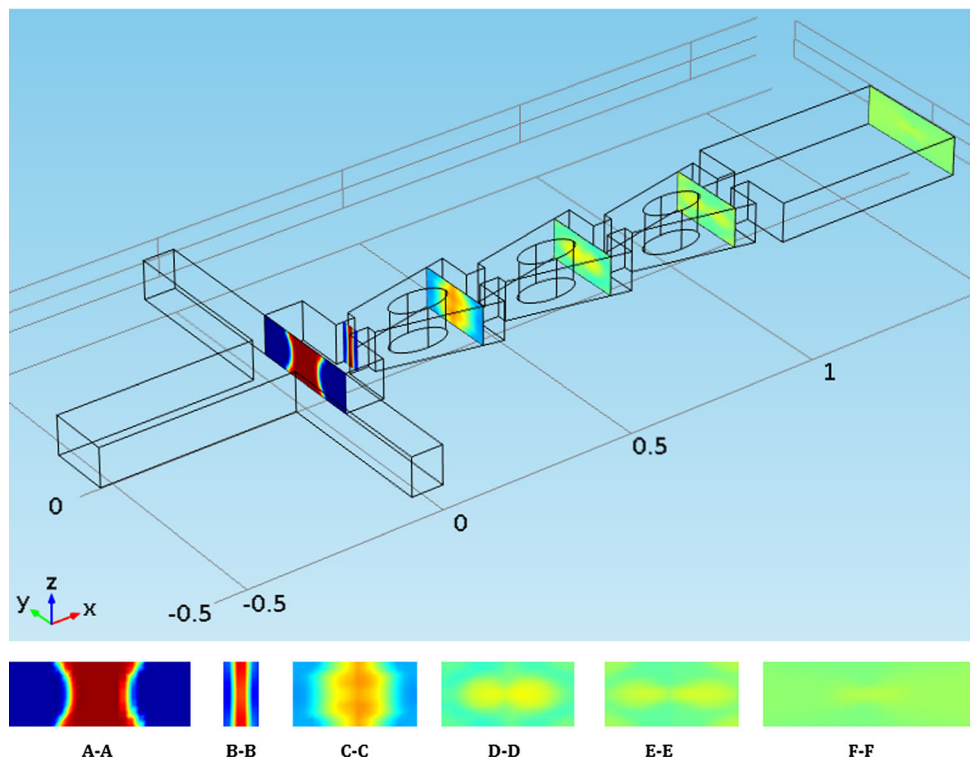


**Fig. 8** Ethanol mass fraction profiles on six planes for EB-TSAR with divergence angle,  $2\theta = 12^\circ$  for  $Re = 45$



flow which in turn increase the interfacial area of the fluid streams. Consequently, facilitating faster diffusion and an improvement in mixing. At very low  $Re$  i.e.  $Re = 0.1$ , the mixing is dominated by molecular diffusion and mixing index value is around 1 for all cases. However, with an

increase in Reynolds and Peclet numbers, the residence time decreases considerably. For example, at  $Re = 5$ , the mixing index decreases considerably, this due to the incomplete formation of separation vortices. The convection dominates the mass transfer process at  $Re > 5$ . By

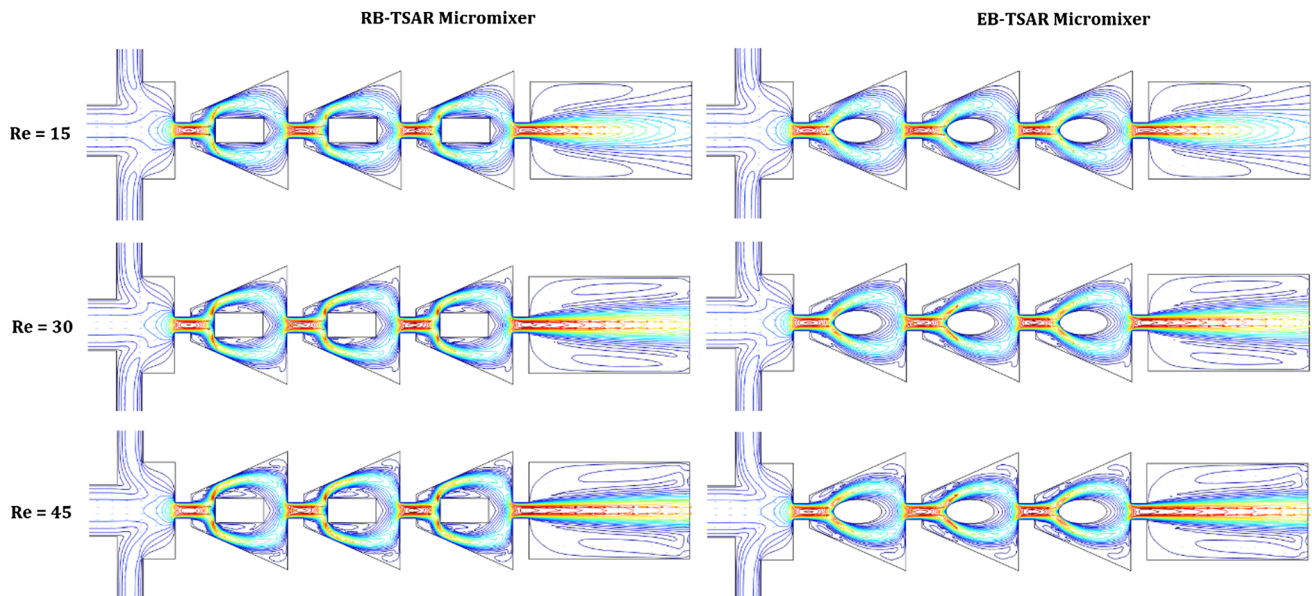


**Fig. 9** Velocity field and velocity magnitude for RB-TSAR and EB-TSAR micromixers with  $20 = 24^\circ$  at  $Re = 15, 30$  and  $45$

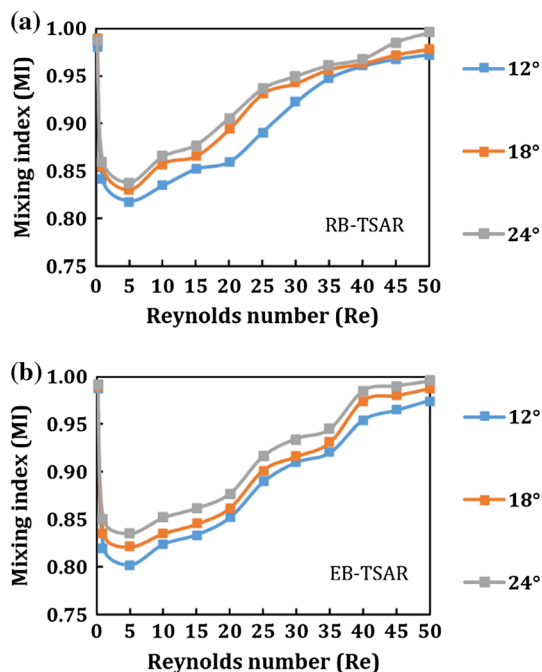


**Fig. 10** Variation of the mixing index at the exit plane **a** RB-TSAR micromixer and **b** EB-TSAR micromixer for  $Re$  in the range  $0.1\text{--}50$

increasing Reynolds number in the range  $10\text{--}50$ , the intensified secondary motion and circulation in the flow due to the baffles enhances the mixing performance.

It can be observed that the mixing index increases with increase in axial distance in the direction of the flow for both designs. For RB-TSAR micromixer, the mixing index at  $0.75$  mm distance from the confluence point for  $Re = 0.1, 30$  and  $45$  is above  $0.80$ , which also fulfills the design

requirements of the micromixer (Nguyen and Wereley 2006) and the mixing index at  $0.75$  mm distance from the confluence point is below  $0.80$  for  $Re = 1, 5$  and  $15$  as shown Fig. 11a–c for RB-TSAR micromixer.

For EB-TSAR micromixer, the mixing index at  $1.1$  mm distance from the confluence point for  $Re = 0.1, 30$  and  $45$  is above  $0.80$ , which also fulfills the design requirements of the micromixer, and the mixing index at  $Re = 1, 5$  and  $15$  is below  $0.80$  as shown in Fig. 12a–c for EB-TSAR micromixer. This change in trend is observed due the shape of the baffle. Thus RB-TSAR micromixer shows better mixing index even at  $0.75$  mm distance from the confluence point when compared with EB-TSAR micromixer.

#### 4.2.2 Pressure drop

In respect of Lab-On-a-Chip (LOC) applications, pressure drop is one of vital operational parameter. The relationship between Reynolds number and pressure drop for RB-TASR and EB-TSAR micromixers is presented Fig. 13. The observed trends for pressure drop indicate that the pressure drop increases with the increase in  $Re$ , which results in enriched mixing. A linear relationship between Reynolds number and pressure drop has been observed for both design configurations. In the micromixer design configurations studied here it is observed that the pressure drop in EB-TSAR micromixer is less than that of RB-TSAR micromixer. This reduced pressure drop EB-TSAR micromixer is due to smooth curves and there is no sharp turn in the geometry of elliptical baffles unlike rectangular baffles.

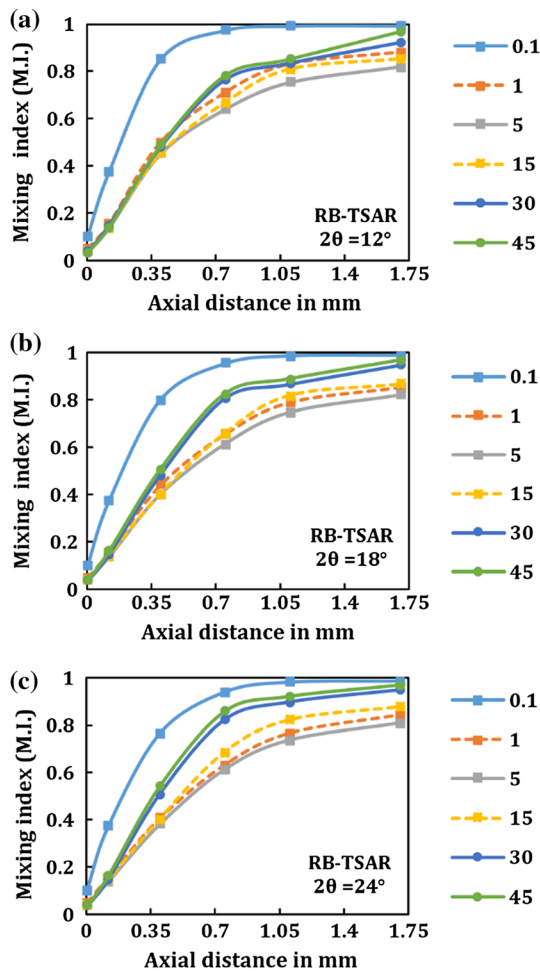


**Fig. 11** Progressive mixing index as a function of stream wise length and divergence angle for RB-TSAR micromixer **a**  $2\theta = 12^\circ$ , **b**  $2\theta = 18^\circ$  and **c**  $2\theta = 24^\circ$  for  $Re = 0.1, 1, 5, 15, 30$  and  $45$

### 4.2.3 Performance index

The ratio of the mixing index to the pressure drop is known as performance index. This is a good measure to evaluate the overall performance of micromixer. High value PI signifies better overall performance. The computed values of PI are depicted in Table 6. The Reynolds number, divergence angle of diffuser mixing element and shape of baffle influence significantly on the performance index. The performance index decreases with the increase of Re numbers and it increases with increase the divergence angle in case of both design configurations. The performance indices in case of EB-TSAR are higher than that of RB-TSAR micromixers at all Reynolds number studied here. This enhanced performance is due to the reduced pressure drop in case EB-TSAR as a result of profile of elliptical baffle.

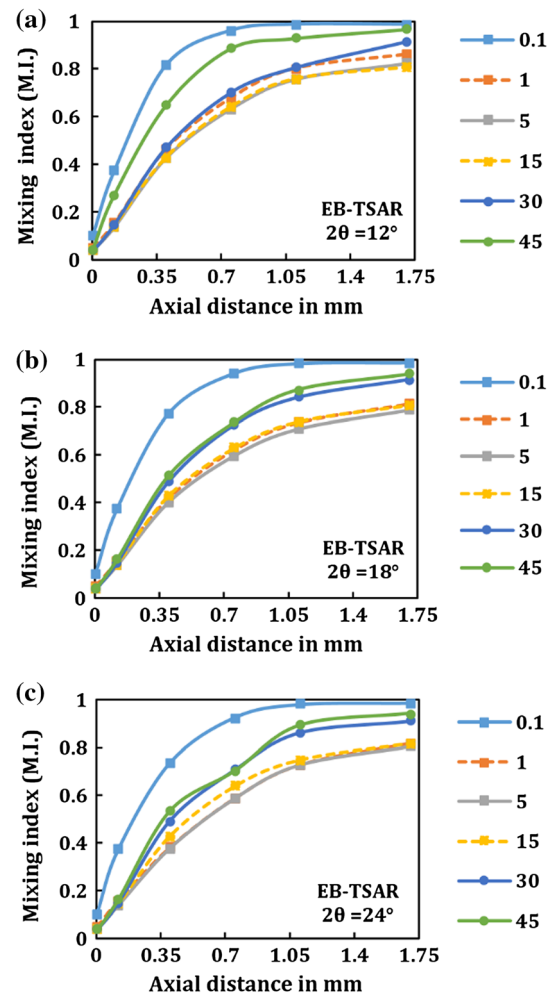


**Fig. 12** Progressive mixing index as a function of stream wise length and divergence angle for EB-TSAR micromixer **a**  $2\theta = 12^\circ$ , **b**  $2\theta = 18^\circ$  and **c**  $2\theta = 24^\circ$  for  $Re = 0.1, 1, 5, 15, 30$  and  $45$

### 4.2.4 Mixing energy cost

The mixing energy cost represents overall better mixing performance. Its low values represent indicate that the particular micromixer has better mixing performance. The comparison of mixing energy costs required for RB-TSAR and EB-TSAR micromixers is depicted in Table 7. From the detailed flow feature analysis, it is noticed that the transverse flow and dean vortices and separation vortices are caused by the comprehensive effects of diffuser elements and baffles wherein transverse flow is caused by splitting of fluid stream as a result of baffle and dean vortices and separation vortices are caused by baffle shape. Further, the intensity of vortices generation is greatly influenced by shape of the baffle. The shape of baffles in the RB-TSAR and EB-TSAR has a significant influence on the pressure drop which ultimately controls the mixing energy cost. The energy input that is used for the mixing process is directly related to the pressure drop. Wherein,

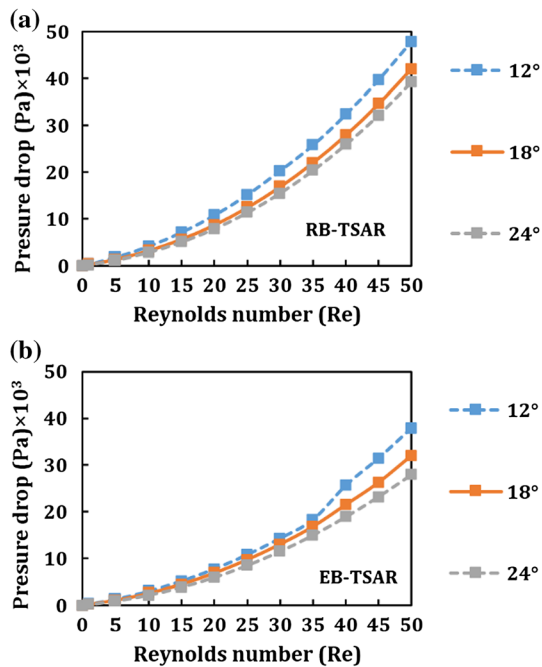


**Fig. 13** Pressure drop as a function of Reynolds number **a** RB-TSAR micromixer and **b** EB-TSAR micromixer

the curved shape of elliptical baffle creates more dean vortices and separation vortices. This curved shape of baffle also helps to reduce pressure drop which in turn reduces mixing energy cost required for the EB-TASR micromixer as compared to the RB-TSAR micromixer. At  $Re = 50$  and  $2\theta = 12^\circ$ , the mixing energy cost required for EB-TSAR is  $257.1513 \mu\text{W}$  whereas the mixing energy cost required to run RB-TSAR is  $322.6392 \mu\text{W}$  which is around 20.29% higher than that of EB-TSAR. Similarly, at  $Re =$

50 the mixing energy costs required for RB-TSAR with  $2\theta = 18^\circ$  and  $2\theta = 24^\circ$  are around 23.29% and 19.53% higher than that of EB-TSAR.

## 5 Conclusions

In this study, a number of CFD simulations were performed to evaluate mixing performance of two micromixer design configurations. The CFD based results showed that the mixer efficiently stirs the fluids, generates secondary vortex flows in the microchannels which results in higher mixing index. The results also reveal that baffles can break the fluid streams, produce fluid convection and increase the contact area of the fluid by folding and deflecting fluid streams which in turn helps to improve the mixing index. At  $Re = 0.1$ , the mixing index and performance index are higher with minimal mixing energy cost. The results of mixing index at  $Re = 5$  for both micromixer design configurations show a considerable decrease in mixing index due less residence time as well as no formation of dean and separation vortices. The Dean and separation vortices play significant role in mixing enhancement which results in better mixing index in short mixing length. The strength of Dean and separation vortices is more in EB-TSAR micromixer as compared to the RB-TSAR micromixer. This variation in performance is due to baffle geometry. The mixing index higher than 0.85 for  $Re$  values in the range 10–50 for both micromixer design configurations which also fulfill design criteria for the micromixers (Nguyen and Wereley 2006).

It is found that EB-TSAR micromixer yields superior mixing index, performance index and mixing energy cost

**Table 6** Performance index of micromixers

Reynolds number (Re)	Performance index per unit pressure drop					
	Divergence angle ( $2\theta$ )					
	RB-TSAR micromixer			EB-TSAR micromixer		
	$12^\circ$	$18^\circ$	$24^\circ$	$12^\circ$	$18^\circ$	$24^\circ$
0.1	2.96E-02	3.99E-02	4.64E-02	3.99E-02	4.87E-02	5.35E-02
1	2.62E-03	3.43E-03	3.94E-03	3.46E-03	3.99E-03	4.41E-03
5	4.52E-04	6.00E-04	6.82E-04	6.14E-04	7.06E-04	7.85E-04
10	2.01E-04	2.67E-04	3.05E-04	2.71E-04	3.14E-04	3.51E-04
15	1.20E-04	1.54E-04	1.74E-04	1.56E-04	1.79E-04	1.91E-04
20	7.98E-05	1.03E-04	1.15E-04	1.09E-04	1.25E-04	1.30E-04
25	5.88E-05	7.50E-05	8.26E-05	8.23E-05	9.27E-05	9.50E-05
30	4.55E-05	5.62E-05	6.13E-05	6.39E-05	7.03E-05	7.12E-05
35	3.68E-05	4.34E-05	4.72E-05	5.08E-05	5.51E-05	5.54E-05
40	2.97E-05	3.45E-05	3.73E-05	3.77E-05	4.43E-05	4.44E-05
45	2.44E-05	2.80E-05	3.01E-05	3.07E-05	3.62E-05	3.66E-05
50	2.03E-05	2.30E-05	2.48E-05	2.55E-05	3.01E-05	3.08E-05

**Table 7** Mixing energy cost of micromixers

	Reynolds number (Re)	Mixing energy cost in $\mu\text{W}$					
		Divergence angle ( $2\theta$ )					
		RB-TSAR micromixer			EB-TSAR micromixer		
		12°	18°	24°	12°	18°	24°
0.1	0.0004	0.0003	0.0003	0.0003	0.0003	0.0002	
1	0.0500	0.0382	0.0333	0.0378	0.0328	0.0297	
5	1.4495	1.0909	0.9603	1.0667	0.9267	0.8346	
10	6.5020	4.9040	4.2967	4.8328	4.1662	3.7329	
15	16.3875	12.7826	11.2727	12.5771	10.9688	10.2599	
20	32.7985	25.4565	22.7039	24.1287	20.9199	20.1915	
25	55.6465	43.6683	39.6111	39.7636	35.3013	34.4563	
30	86.4159	69.9601	64.0699	61.5075	55.8844	55.1685	
35	124.6369	105.5460	97.0053	90.2723	83.2107	82.7442	
40	176.3603	152.0012	140.2383	139.0798	118.3214	117.9885	
45	241.7658	210.6136	195.6040	192.1445	162.5789	161.0395	
50	322.6392	284.2578	263.8822	257.1513	217.2850	212.3451	

than that of RB-TSAR due to the intensified secondary flow generated by curves elliptical baffle and separation vortices which leads to a chaotic flow regime. Further, EB-TSAR has lower pressure drop compared with the RB-TSAR micromixer. This decrease in pressure drop is due to the shape of elliptical baffle wherein the fluids streams experience less resistance to flow. It is also noted that with increased divergence angle the mixing index generally increases with decrease in the pressure drop as well.

Another important factor responsible for homogeneous mixing is variations in the magnitude of fluid velocity due to divergence section of diffuser shaped mixing element and narrow constriction channel used to connect two diffuser shaped mixing element. As a result, the mixing index is enhanced greatly and the complete mixing is achieved at a short length. Furthermore, RB-TSAR and EB-TSAR micromixers have a small footprint, thus can be easily integrated into Lab-On-a-Chip for various chemical and biological applications.

The proposed study is focused on detailed flow physics analysis and performance analysis based on four parameters viz. mixing index, pressure drop, performance index and mixing energy cost.

## 6 Future studies

As the mixing characteristics of micromixer is closely affected by geometrical variations of micromixers. In view of the enhanced mixing characteristics or capability of the proposed micromixer designs, we intend to perform design optimization of three inlet-based short mixing length micromixers. The influence of shape of mixing element and

baffle/obstacle, aspect ratio of baffle/obstacle, position of obstacles (i.e. at the start, at the middle and at the end of mixing element) etc. on mixing characteristics can be studied. One of the multi-objective optimization method i.e. Taguchi-based Grey Relational Analysis (GRA) and in-depth flow feature analysis will be performed to identify the optimal micromixer design configuration.

## References

- Afzal A, Kim KY (2012) Passive split and recombination micromixer with convergent–divergent walls. *Chem Eng J* 203:182–192
- Ansari MA, Kim KY (2010) Mixing performance of unbalanced split and recombine micromixers with circular and rhombic sub-channels. *Chem Eng J* 162(2):760–767
- Bothe D, Stemich C, Warnecke HJ (2006) Fluid mixing in a T-shaped micro-mixer. *Chem Eng Sci* 61(9):2950–2958
- Chen X, Shen J (2017) Numerical and experimental investigation on splitting-and-recombination micromixer with E-shape mixing units. *Microsyst Technol* 23(10):4671–4677
- Chen X, Zhao Z (2017) Numerical investigation on layout optimization of obstacles in a three-dimensional passive micromixer. *Anal Chim Acta* 964:142–149
- Chen X, Li T, Hu Z (2016a) A novel research on serpentine microchannels of passive micromixers. *Microsyst Technol* 23(7):2649–2656
- Chen X, Li T, Zeng H, Hu Z, Fu B (2016b) Numerical and experimental investigation on micromixers with serpentine microchannels. *Int J Heat Mass Transf* 98:131–140
- Chen X, Zhang Z, Yi D, Hu Z (2017) Numerical studies on different two-dimensional micromixers basing on a fractal-like tree network. *Microsyst Technol* 23(3):755–763
- Cheri MS, Latifi H, Moghaddam MS, Shahraki H (2013) Simulation and experimental investigation of planar micromixers with short-mixing-length. *Chem Eng J* 234:247–255
- Chung CK, Shih TR (2007) A rhombic micromixer with asymmetrical flow for enhancing mixing. *J Micromech Microeng* 17(12):2495



- Chung YC, Hsu YL, Jen CP, Lu MC, Lin YC (2004) Design of passive mixers utilizing microfluidic self-circulation in the mixing chamber. *Lab Chip* 4(1):70–77
- Chung CK, Shih TR, Chang CK, Lai CW, Wu BH (2011) Design and experiments of a short-mixing-length baffled microreactor and its application to microfluidic synthesis of nanoparticles. *Chem Eng J* 168(2):790–798
- Cortes-Quiroz CA, Zangeneh M, Goto A (2009) On multi-objective optimization of geometry of staggered herringbone micromixer. *Microfluid Nanofluid* 7(1):29–43
- Cortes-Quiroz CA, Azarbadegan A, Zangeneh M (2014) Evaluation of flow characteristics that give higher mixing performance in the 3-D T-mixer versus the typical T-mixer. *Sens Actuators B Chem* 202:1209–1219
- Falk L, Commenge JM (2010) Performance comparison of micromixers. *Chem Eng Sci* 65(1):405–411
- Galletti C, Roudgar M, Brunazzi E, Mauri R (2012) Effect of inlet conditions on the engulfment pattern in a T-shaped micro-mixer. *Chem Eng J* 185:300–313
- Gidde RR, Pawar PM (2019) Flow feature analysis of T-junction wavy micromixer for mixing application. *Int J Chem React Eng*. <https://doi.org/10.1515/ijcre-2018-0306>
- Gidde RR, Pawar PM, Ronge BP, Misal ND, Kapurkar RB, Parkhe AK (2018a) Evaluation of the mixing performance in a planar passive micromixer with circular and square mixing chambers. *Microsyst Technol* 24(6):2599–2610
- Gidde RR, Shinde AB, Pawar PM, Ronge BP (2018b) Design optimization of a rectangular wave micromixer (RWM) using Taguchi based grey relational analysis (GRA). *Microsyst Technol* 24(9):3651–3666
- Gidde RR, Pawar PM, Ronge BP, Shinde AB, Misal ND, Wangikar SS (2018c) Flow field analysis of a passive wavy micromixer with CSAR and ESAR elements. *Microsyst Technol* 25(3):1017–1030
- Gidde RR, Pawar PM, Gavali SR, Salunkhe SY (2019) Flow feature analysis of an eye shaped split and collision (ES-SAC) element based micromixer for lab-on-a-chip application. *Microsyst Technol*. <https://doi.org/10.1007/s00542-018-4271-x>
- Gigras A, Pushpavanam S (2008) Early induction of secondary vortices for micromixing enhancement. *Microfluid Nanofluid* 5(1):89–99
- Goet G, Baier T, Hardt S (2009) Micro contactor based on isotachophoretic sample transport. *Lab Chip* 9(24):3586–3593
- Hardt S, Drese K, Hessel V, Schönfeld F (2004) Passive micro mixers for applications in the micro reactor and  $\mu$ TAS field. In: 2nd international conference on microchannels and minichannels, American Society of Mechanical Engineers, pp 45–55
- Hossain S, Kim KY (2014) Mixing analysis of passive micromixer with unbalanced three-split rhombic sub-channels. *Micromachines* 5(4):913–928
- Hossain S, Lee I, Kim SM, Kim KY (2017) A micromixer with two-layer serpentine crossing channels having excellent mixing performance at low Reynolds numbers. *Chem Eng J* 327:268–277
- Huang SW, Wu CY, Lai BH, Chien YC (2017) Fluid mixing in a swirl-inducing microchannel with square and T-shaped cross-sections. *Microsyst Technol* 23:1971–1981
- Jain M, Rao A, Nandakumar K (2013) Numerical study on shape optimization of groove micromixers. *Microfluid Nanofluid* 15(5):689–699
- Kim DS, Lee SH, Kwon TH, Ahn CH (2005) A serpentine laminating micromixer combining splitting/recombination and advection. *Lab Chip* 5(7):739–747
- Kuo JN, Li YS (2017) Centrifuge-based micromixer with three-dimensional square-wave microchannel for blood plasma mixing. *Microsyst Technol* 23:2343–2354
- Liu M (2011) Computational study of convective–diffusive mixing in a microchannel mixer. *Chem Eng Sci* 66(10):2211–2223
- Nguyen NT, Wereley S (2006) Fundamentals and applications of microfluidics. Artech House, Boston, pp 293–341
- Nguyen NT, Wu Z (2004) Micromixers—a review. *J Micromech Microeng* 15(2):R1
- Oh DW, Jin JS, Choi JH, Kim HY, Lee JS (2007) A microfluidic chaotic mixer using ferrofluid. *J Micromech Microeng* 17(10):2077
- Okuducu M, Aral M (2018) Performance analysis and numerical evaluation of mixing in 3-D T-shape passive micromixers. *Micromachines* 9(5):210
- Okuducu MB, Aral MM (2019) Computational evaluation of mixing performance in 3-D swirl-generating passive micromixers. *Processes* 7(3):121
- Ortega-Casanova J (2016) Enhancing mixing at a very low Reynolds number by a heaving square cylinder. *J Fluids Struct* 65:1–20
- Posner JD, Santiago JG (2006) Convective instability of electrokinetic flows in a cross-shaped microchannel. *J Fluid Mech* 555:1–42
- Pradeep A, Raveendran J, Ramachandran T, Nair BG (2016) Computational simulation and fabrication of smooth-edged passive micromixers with alternately varying diameter for efficient mixing. *Microelectron Eng* 165:32–40
- Roudgar M, Brunazzi E, Galletti C, Mauri R (2012) Numerical study of split T-micromixers. *Chem Eng Technol* 35(7):1291–1299
- Sahu PK, Golia A, Sen AK (2013) Investigations into mixing of fluids in microchannels with lateral obstructions. *Microsyst Technol* 19:493–501
- Sarkar S, Singh KK, Shankar V, Shenoy KT (2015) CFD simulations to study the effects of wall protrusions on microfluidic mixing. *J Micromech Microeng* 25(8):084008
- Shah I, Kim SW, Kim K, Doh YH, Choi KH (2019) Experimental and numerical analysis of Y-shaped split and recombination micromixer with different mixing units. *Chem Eng J* 358:691–706
- Shih TR, Chung CK (2008) A high-efficiency planar micromixer with convection and diffusion mixing over a wide Reynolds number range. *Microfluid Nanofluid* 5(2):175–183
- Suh YK, Kang S (2010) A review on mixing in microfluidics. *Micromachines* 1:82–111
- The HL, Ta BQ, Thanh HL, Dong T, Thoi TN, Karlsen F (2015a) Geometric effects on mixing performance in a novel passive micromixer with trapezoidal-zigzag channels. *J Micromech Microeng* 25:094004
- The HL, Thanh HL, Dong T, Ta BQ, Tran-Minh N, Karlsen F (2015b) An effective passive micromixer with shifted trapezoidal blades using wide Reynolds number range. *Chem Eng Res Des* 93:1–11
- Tran-Minh N, Dong T, Karlsen F (2014) An efficient passive planar micromixer with ellipse-like micropillars for continuous mixing of human blood. *Comput Methods Progr Biomed* 117(1):20–29
- Wang H, Iovenitti P, Harvey E, Masood S (2002) Optimizing layout of obstacles for enhanced mixing in microchannels. *Smart Mater Struct* 11(5):662
- Xia GD, Li YF, Wang J, Zhai YL (2016) Numerical and experimental analyses of planar micromixer with gaps and baffles based on field synergy principle. *Int Commun Heat Mass Transfer* 71:188–196
- Yang Z, Goto H, Matsumoto M, Maeda R (2000) Active micromixer for microfluidic systems using lead-zirconate-titanate (PZT) generated ultrasonic vibration. *ELECTROPHOR Int J* 21(1):116–119
- Yaralioglu GG, Wiygant IO, Marentis TC, Khuri-Yakub BT (2004) Ultrasonic mixing in microfluidic channels using integrated transducers. *Anal Chem* 76(13):3694–3698

**Publisher's Note** Springer Nature remains neutral with regard to jurisdictional claims in published maps and institutional affiliations.